We are IntechOpen,
the world's leading publisher of
Open Access books
Built by scientists, for scientists

4,800
Open access books available

122,000
International authors and editors

135M
Downloads

Our authors are among the

154
Countries delivered to

TOP 1%
most cited scientists

12.2%
Contributors from top 500 universities

CLARIVATE ANALYTICS
BOOK CITATION INDEX
INDEXED

WEB OF SCIENCE™

Selection of our books indexed in the Book Citation Index
in Web of Science™ Core Collection (BKCI)

Interested in publishing with us?
Contact book.department@intechopen.com

Numbers displayed above are based on latest data collected.
For more information visit www.intechopen.com

Chapter

Real-Time Particle Radiography by Means of Scintillating Fibers Tracker and Residual Range Detectors

Domenico Lo Presti, Giuseppe Gallo, Danilo Luigi Bonanno,
Daniele Giuseppe Bongiovanni, Fabio Longhitano and
Santo Reito

Abstract

In this chapter, a detailed description of the construction and the procedure for the measurement of performances of a charged particle imaging system is given. Such a system can be realized by the combined use of a position sensitive detector and a residual range detector. The position sensitive detector is made up of two superimposed and right-angled planes, each of which subsists of two layers of pre-aligned and juxtaposed scintillating fibers. The selected 500 μm square section fibers are optically coupled to two silicon photomultiplier arrays adopting a channel reduction system patented by the Istituto Nazionale di Fisica Nucleare. The residual range detector consists of 60 parallel layers of the same fibers used in the position detector, each of which is optically coupled to a channel of silicon photomultiplier array by means of two wavelength-shifting fibers. The sensitive area of both detectors is 90×90 mm^2. The performance of the prototypes was tested in different facilities with protons and carbon ions at energy up to about 250 MeV and rate up to about 10^9 particles per second. The comparison between simulations and measurements confirms the validity of this system. Based on the results, a future development is a real-time radiography system exploiting high-intensity pencil beams and real-time treatment plan verification.

Keywords: real-time particle radiography, innovative detector readout strategy, beam monitoring, scintillating optical fibers, treatment plan verification

1. Introduction

Hadron therapy is a promising alternative in treatment of tumors, because it is one of the most effective techniques of external radiation therapy, which allows killing tumor cells while leaving almost intact the surrounding issue. In order to achieve the maximum effectiveness, high precision is needed in dose delivery, which requires a real-time adequate quality control of the beam parameters (position, profile, fluence, energy) combined with the precise measurement of patient positioning [1, 2]. QBeRT is a particle tracking system [3] and consists of a position-sensitive

detector (PSD) and a residual range detector (RRD) (see **Figure 1**). The main parts of this system are detectors expressly designed to achieve high-resolution imaging, high-resolution residual range measurement, large sensitive area, and high-rate beam compliance. The QBeRT system performs all these tasks and, advantageously, requires a low number of readout channels, making possible the reduction of the complexity and cost of the electronic data acquisition (DAQ) chain, by means of a readout channel reduction system patented by Istituto Nazionale di Fisica Nucleare (INFN) [4]. Both detectors, PSD and RRD, are able to work in imaging conditions, with particle rate up to 10^6 particles per second, and in therapy conditions (up to 10^9 particles per second). In imaging condition, the system is capable to realize a particle radiography and permits a real-time monitoring of the patient position in treatment room. In therapy condition, the PSD acts as a profilometer, detecting the position, the profiles, and the fluence of the beam. The combined use of the information measured by the PSD and the RRD allows to check the treatment plan in real time. The design of both detectors is based on scintillating optical fibers (SciFi) with 500 µm nominal square section.

The working principle of the scintillating optical fibers is schematized in **Figure 2**. SciFi consist of a polystyrene-based core and a PMMA cladding. The scintillating core is a mix of polystyrene and fluorescent dopants selected to produce the scintillation light when a particle releases energy in it and sets the optical characteristics for light propagation in the fiber. Scintillation light is produced isotropically but only a portion of these photons, in the two opposite directions along the fiber, can propagate by total internal reflection (TIR) mechanism. Multi-clad fibers have a second layer of cladding that has an even lower refractive index and permits TIR at a second boundary. External EMA is an optional external layer used to eliminate optical cross talk. SciFi sizes range from 0.25 to 5 mm square or round cross-sections and available in canes, spools, ribbons, and arrays.

The scintillation light is routed by the SciFi in the PSD, by means of wavelength-shifting fibers in the RRD, toward two silicon photomultiplier (SiPM) arrays, which output a proportional electric signal. PSD and RRD employ a DAQ chain divided in two sections. The first section consists of the front-end (FE) boards, which process the electric signal from the light sensor and perform the analog-to-digital conversion.

Data from the FE is acquired by a readout (RO) board based on a National Instrument system on module (SoM) for pre-analysis and filtering. The actual readout channel reduction scheme applied to the PSD limits the performances of
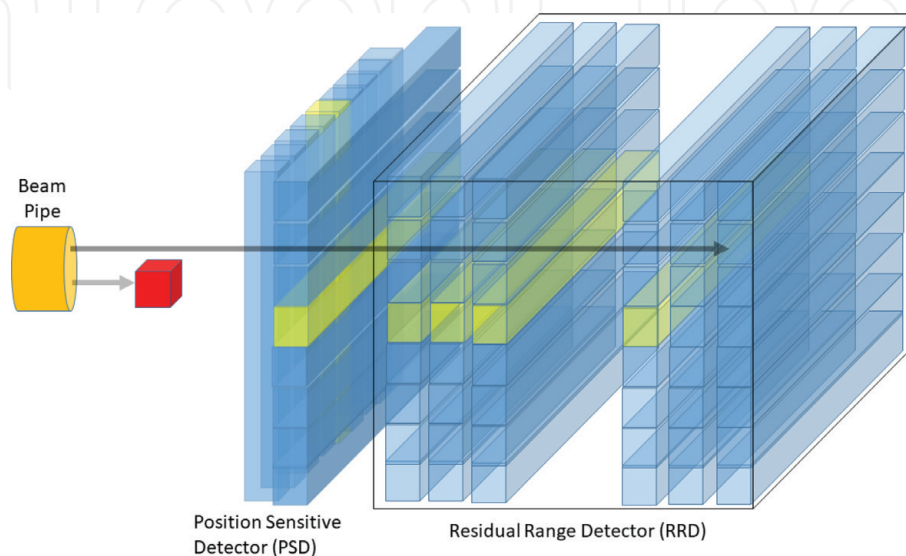

Beam
Pipe

Position Sensitive
Detector (PSD)

Residual Range Detector (RRD)

Figure 1.
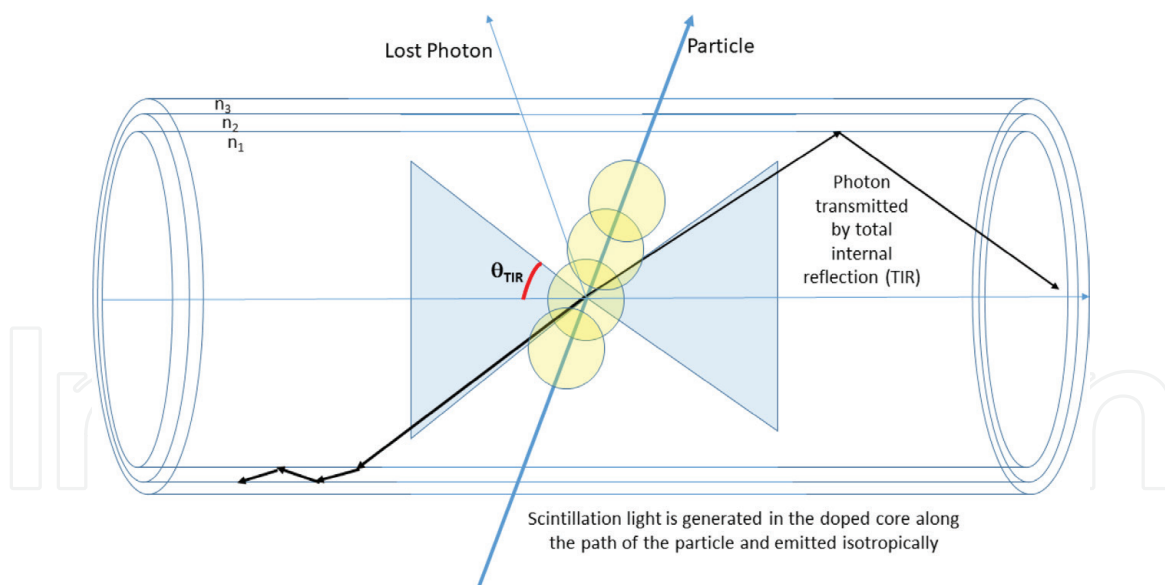*Schematic of the QBeRT proton tracking system.*

Figure 2.
Working principle of the scintillating fibers.

the detector when the beam spot size exceeds about 2 cm. Notice that the choice of the suitable readout channel reduction scheme and the modularity of the detector architecture allows to resize the sensitive area and the maximum beam spot size in order to fit any specific requirement. It is possible to obtain a large area detector (up to 400 × 400 mm^2) covering a range up to 250 MeV protons with high spatial and range resolution (up to 150 and 170 μm, respectively). The detectors described in this chapter have been intensively tested in imaging and therapy (up to 10^9 proton/s) conditions [5] thanks to the collaboration with the colleagues working at CATANA facility (Centro di AdroTerapia ed Applicazioni Nucleari Avanzate at Laboratori Nazionali del Sud-Istituto Nazionale di Fisica Nucleare in Catania), at TIFPA (Trento Institute for Fundamentals Physics Applications) in Trieste, and at CNAO (Centro Nazionale di Adroterapia Oncologica) in Pavia.

2. The position-sensitive detector

The PSD prototype has a sensitive area of 90 × 90 mm^2, which is made of two ribbons, layers of pre-aligned BCF-12 SCIFI, manufactured by Saint-Gobain Crystals, juxtaposed and orthogonally oriented, named the X and Y planes. The SciFi have 500 μm nominal square section. In detail, each single layer is composed of four ribbons of 40 fibers. The ribbons are optically isolated from each other by means of 220-μm-thick black adhesive tape to reduce cross talk between adjacent and overlapped ribbons. Each fiber is coated with white extra mural absorber (EMA) [6] to further reduce the cross talk between individual fibers. Particles intersecting the PSD's sensitive area deposit energy in the fibers which is partially converted in scintillation light. A fraction of this light is channeled in the core and propagated in the fiber toward the photo-sensor. When a particle loses suitable energy in all four SciFi layers, the coordinates of the intersection of its trajectory and the sensitive area can be measured. A picture of PSD detector is shown in **Figure 3**.

The PSD has 640 optical channels (four layers of 160 fibers each). The channel reduction system reduces the number of the readout channels without any data loss or degradation in the position measurement. The readout is performed in time coincidence, strongly reducing the effect of noise and chance coincidences, enhancing at the same time the performances of the system. The working principle of channel
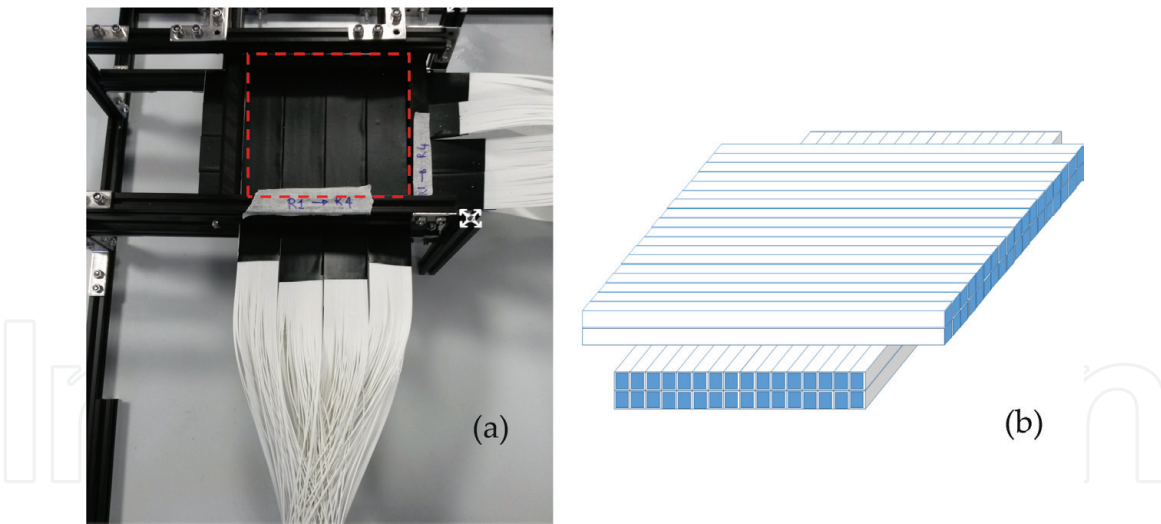
Figure 3.
(a) Picture of PSD detector during the assembly phase. The dashed red box highlights the sensitive area of the detector. (b) A sketch of the arrangement of the four layers is shown.

reduction can be argued by considering a strip detector able to detect one particle at a time. Each strip can be read from both ends, and the signals are grouped following the scheme reported in **Figure 4**, where a two-dimension 16-strip detector is illustrated. All strips are read out, on one end, in m groups of n neighboring strips, named *NeigSet*, while at the other end, the first strips of each group are grouped in *StripSet1*, the second strips of each group in *StripSet2*, and so on to m. The two numbers are not necessarily the same. The minimum number of total channels, obtained by choosing $n = m$, is $4\sqrt{N}$, where N is the total number of strips per layer, X or Y. This implies that the number of readout channels on the second side is equal to the number of fibers per channel on the first side. A particle crossing one
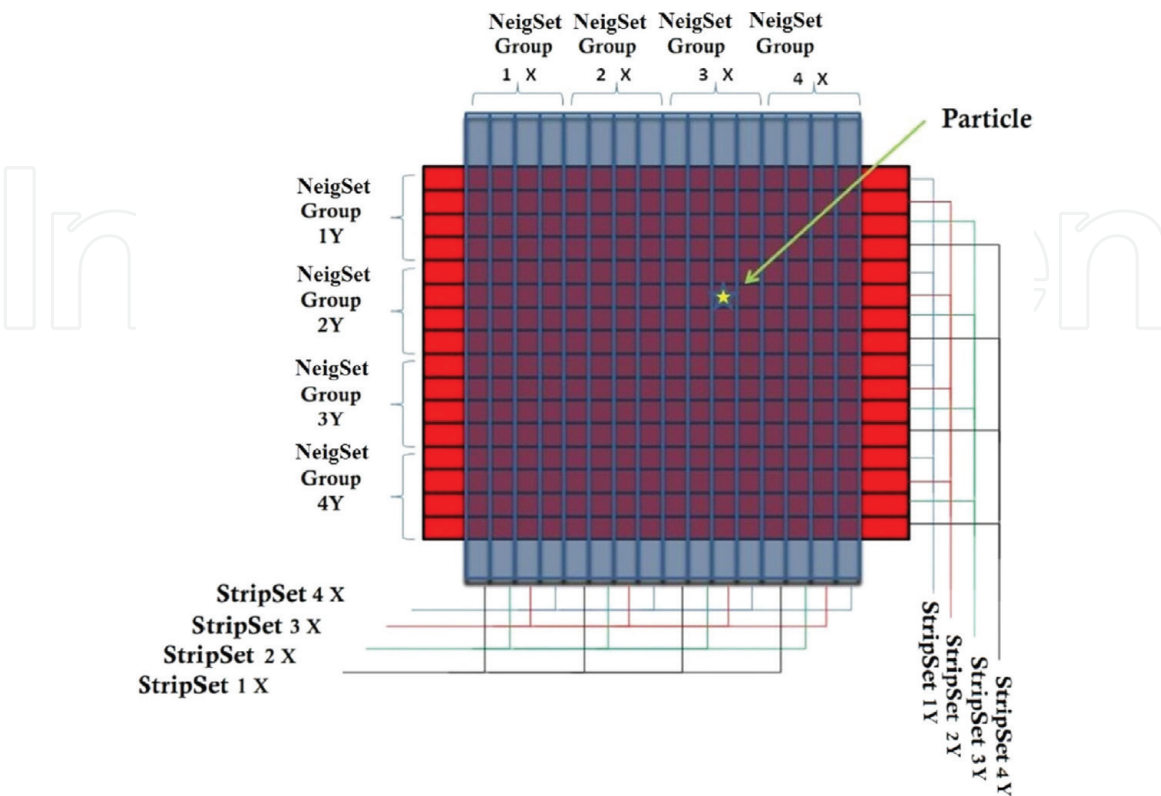

Figure 4.
An example of the application of the channel reduction scheme to a two-dimension 16-strip detector.

strip generates a signal at both ends of the fiber. Then, we have a signal from the ith *NeigSet* group and another from the jth *StripSet* that univocally identifies the $Strip_{hit}$ hit, according to equation (1):

$$Strip_{hit} = (i - 1) \cdot n + j. \qquad (1)$$

The developed readout scheme reduces the number of readout channels to 16, instead of 32 channels without the application of the compression. When N is large, the reduction factor becomes important, allowing a compact and low-cost real-time acquisition. Notice that to reconstruct the point where the particle crosses the detector (event), an energy release in both planes is needed. In the PSD, readout occurs in time coincidence between the two layers of fibers for each plane. The channel reduction system can read the signal from the whole detector with only 112 channels (less than a fifth respect to the 640 total channels). Each of the 56 optical channels per plane is optically coupled to one of the 64 channels of a SiPM array. For a detailed description of the readout channel reduction system, see Refs. [7–10].

2.1 The PSD DAQ chain

As previously stated, the signals from the SiPM arrays are acquired by a DAQ chain divided in two main sections. The first section consists of the FE electronics which operate the analog-to-digital conversion. The digital-encoded data output from the FE is sent to the RO board which hosts a system on module (SoM) manufactured by the National Instrument (NI) for decoding and filtering. The SoM basically consists of a field-programmable gate array (FPGA) and a real-time processor, communicating by means of a direct memory access (DMA) data bus. The real-time processor has gigabit Ethernet connection for data transfer toward a PC, where the real-time visualization and storage of the results are accomplished.

Two FE boards, one for each direction, are required. Each FE board hosts a 64-channel SiPM array manufactured by Hamamatsu Photonics, mod. S13361-3050AE-08, with 3×3 mm^2 photosensitive area per channel. These custom designed boards amplify and filter the analog signals from each SiPM array channel and compare them, by means of an array of fast comparators, to an individual threshold, remotely settable by a DAC. An individual threshold per channel is useful to compensate the unavoidable mismatch of the SiPMs gain and of the optical coupling of SiPM to fibers. The output of each FE board is an asynchronous digital data bus of 56 bits which represents the status of the SiPM signals and is acquired by the NI SoM on the RO board. The FPGA samples the FE output at high frequency, up to 250 MHz. This data is transferred toward the SoM processor via DMA. The processor applies real-time filtering algorithms and, after discarding the spurious events, reconstructs the impact point of the particles. The SoM's FPGA can be programmed via a graphical approach by means of the LabVIEW platform. The LabVIEW platform also manages the entire acquisition chain and data processing in real time.

3. The residual range detector

The RRD prototype is a stack of 60 layers, 90×90 mm^2 area. Any layer is a ribbon of 180 BCF-12 SciFi. A picture of the detector is shown in **Figure 5(a)**. The ribbons are oriented horizontally and optically coupled at both ends to 1 mm square section wavelength-shifting fibers (WLS), see **Figure 5(b)** and **(c)**. To avoid optical cross talk between adjacent RRD layers, which would degrade range resolution and therefore energy measurement, each layer is optically isolated from the others by
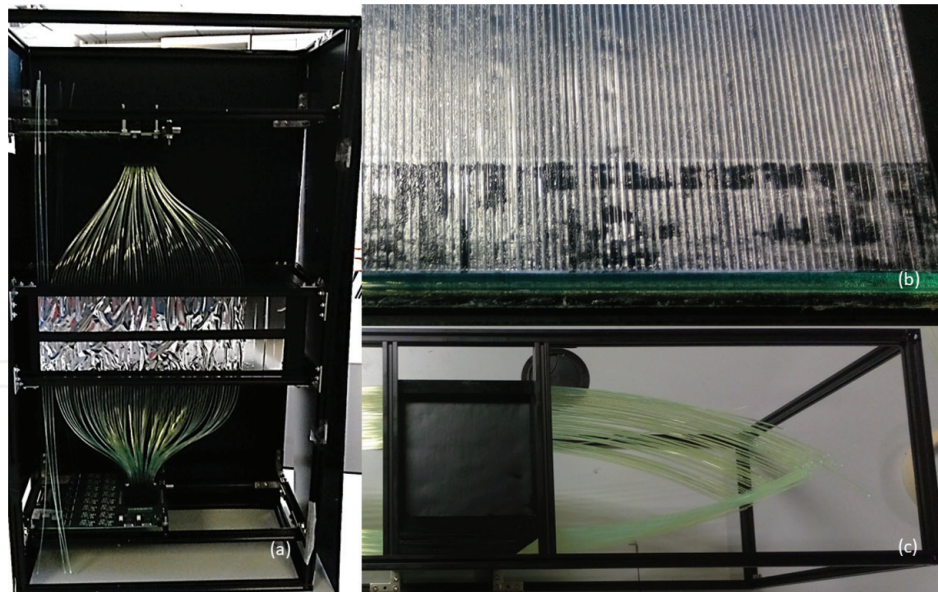
Figure 5.
(a) View of the RRD prototype. (b) Detail of the optical coupling between SciFi and WLS fibers in a RRD layer. (c) View of the sensitive area of the RRD.

means of 100 μm black adhesive film. The SciFi used in the RRD are not coated with EMA because cross talk between adjacent fibers in the same layer does not affect detector resolution. The scintillation light produced in each layer at the passage of the particle is partially absorbed, reemitted, and channeled by the WLS. The two WLS coupled to a layer transfer the collected light to a channel of a SiPM array. The FE output is, then, processed by the DAQ chain. The SiPM array and the DAQ chain are identical to those used in the PSD described in the previous section.

A charged particle crossing the RRD passes through a number of layers as a function of its initial energy, before stopping. The dose deposited in each layer increases with depth up to the Bragg peak, where the particles produce the maximum amount of scintillation light. This point corresponds approximately to the end of the particles' path in the detector, so, by detecting the layer in which the light signal is the more intense, it is possible to measure their range. The RRD's working principle is reported in **Figure 6**. A calibration of the detector allows to obtain a
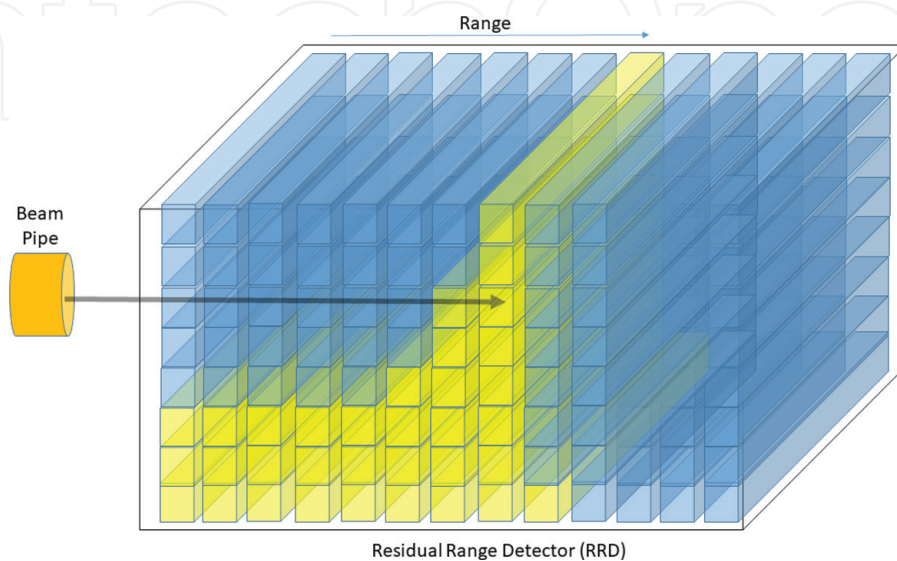

Figure 6.
Working principle of the RRD. In this figure, the height of the yellow column is proportional to the energy released in each layer by a particle crossing the RRD.

range-energy characteristic curve, which can be fitted by a function $R_0 = \alpha E_0^p$. In this way, it is possible to retrieve the initial energy of the particles from the measured range. For the actual RRD, the maximum measurable range was about 36 mm in polystyrene/PVC corresponding to the range of protons with 67 MeV initial energy, but this maximum range can be easily extended up to higher energies by placing a stack of calibrated water-equivalent range shifters between the beam exit and the RRD entry window.

4. Experimental results

Measurements at CATANA were carried out to fully characterize the performance of the prototypes, with protons up to 58 MeV at the output in treatment room. During the last year, other measurements have taken place at TIFPA proton irradiation facility. The spatial resolution of the PSD was measured by means of a calibrated brass collimator applied at the beam pipe exit in the treatment room at CATANA. After data analysis, it is possible to estimate the holes' centers and compare them with the projection of the collimator holes on the detector plane. Then, the mean distances between the reconstructed centers and the collimator hole centers were calculated for each hole, and the mean distance was about 130 μm, comparable with the (a priori) spatial resolution of the PSD, given by 500 μm/$\sqrt{12}$. The maximum spatial resolution is an intrinsic characteristic of the detector, independent of the readout strategy.

In order to calibrate the RRD, several measures of the range have been acquired changing the initial energy of protons. At CATANA facility, the proton beam energy can be passively modulated by placing a different calibrated PMMA range shifter at the beam pipe exit. The energy of the protons at the beam pipe exit was calculated by means of Monte Carlo simulation. The Bragg peak position is not exactly at the real end of the particles' path but just before. It is an experimentally consolidated practice to assume that the particle range measurement corresponds to the distance
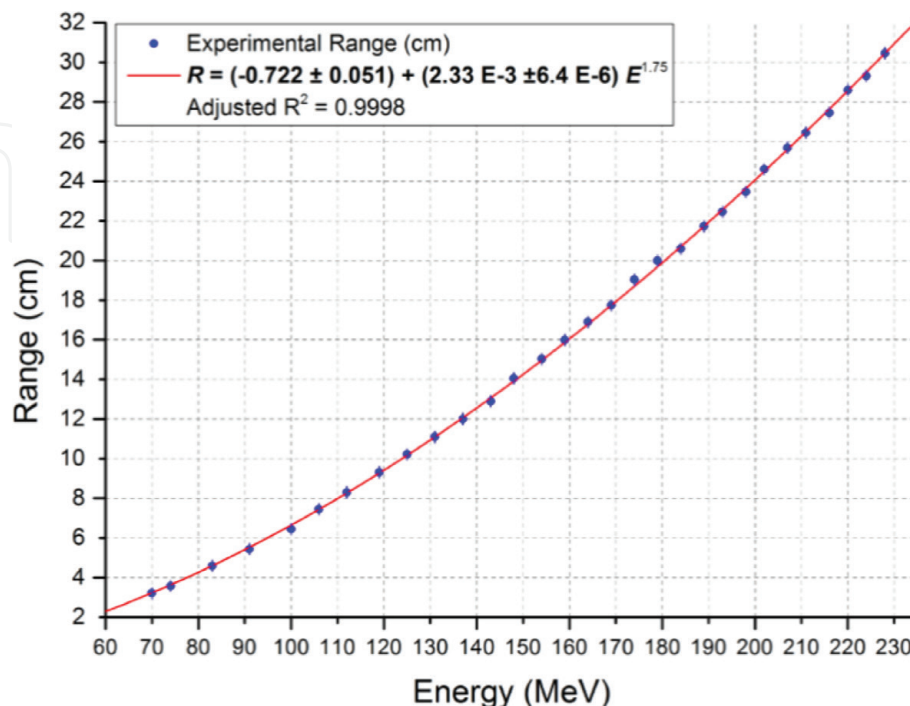

Figure 7.
Measured values of the range vs. the corresponding proton energy at TIFPA and resulting data fit.

from the entrance window where the intensity of the signal is one tenth of its maximum value.

This distance corresponds to the layer on the right of the Bragg peak (or the next layer compared to the incident beam direction). The results of this measurement are compared with the range values calculated by means of a Monte Carlo simulation of the response of the detector. Both data sets were fitted with the power law (Eq. (1)):

$$R = a + b \cdot E^{1.75} \tag{1}$$

where R is the range of the protons in the RRD, E is the kinetic energy at the entrance of the RRD, and a and b are free parameters of fit.

The same measurement was performed at TIFPA with proton energy in the range between 70 and 250 MeV and with a high-intensity beam, up to 10^9 protons per second.

In order to extend the range of the RRD, a series of calibrated water-equivalent range shifters, 10-mm-thick polystyrene slab phantoms was placed in front of the entry window of the RRD every time the energy of the beam exceeded the range of detector alone. In **Figure 7**, the range vs. energy calibration graph, measured at TIFPA, is shown.

5. Beam profile measurement

The PSD can work as a profilometer at rate up to 10^9 particles per second therapy conditions. It is able to measure the size and the position of the beam spot. As a
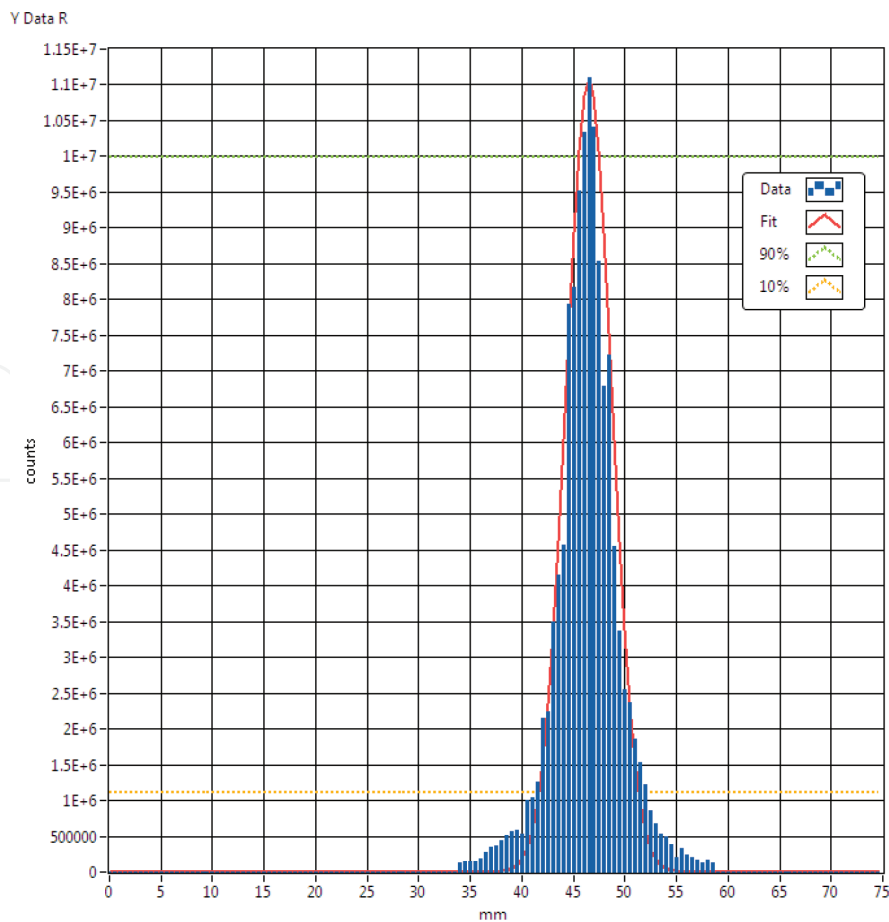

Figure 8.
Examples of Y profile of the proton beam spot at 70 MeV. The calculated Gaussian fit, in red, is superimposed to data.

consequence of the application of the channel reduction system, the beam profile can be reconstructed only if the beam spot size is lower or equal to the width of a ribbon (about 2 cm). The PSD was tested as a profilometer at TIFPA, where the beam optics causes a reduction of the beam spot size with increasing energy. In the test, the PSD worked properly at high energies, as shown in **Figure 8**.

6. The proton radiography

The PSD and RRD have been tested in radiography configuration at CATANA. In this test, the experimental setup is the one previously described, but the two detectors were simultaneously active.

In order to acquire a radiographic image, a range measurement must be performed for each particle crossing the PSD at a given position. Then, data acquisition must run at low beam intensity (imaging conditions, about 10^6 particles per second on average). When a particle causes a quadruple time coincidence in the PSD, the crossing position within the sensitive area is measured, and a trigger signal starts the measurement of the particle range in the RRD. The software analysis associates the positions measured by the PSD to the RRD range measurements event by event. At the end of data acquisition for each pixel, the software analysis calculates the centroid by Gaussian fit of the range measurements distribution corresponding to that pixel. The result of this analysis is, therefore, a 160 × 160 matrix, as many as the PSD pixels, in which each element is the centroid of the range measurement of the particles that have crossed the corresponding pixel. Note that the use of a single PSD placed before the RRD can introduce a not negligible error for the fact that the input and output particle crossing positions through the calibrated target one must necessarily be assumed coincident or
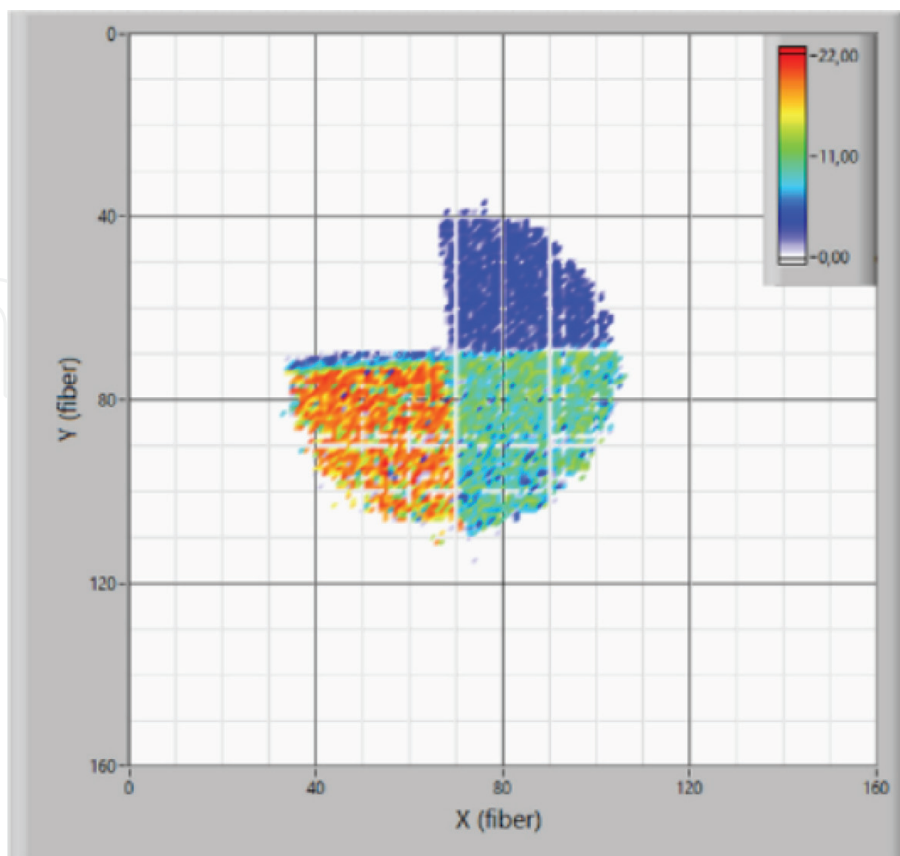

Figure 9.
The radiography of the ladder target with A12 range shifter.

undergone a negligible deflection traversing the medium. This error could be minimized using multiple PSD at different depths in the RRD.

A simple PVC target with the shape of a ladder was designed for the radiography test. Due to the homogeneous density of the target, in the radiography, only the differences in thickness traversed by the protons can be distinguished. The radiography image reported in **Figure 9** refers to a 3.5 cm diameter beam crossing a PMMA range shifter of about 10 mm thickness.

The z value in **Figure 9** is the centroid of the range distribution, expressed in numbers of RRD layers, pixel by pixel. Notice that the empty quarter-circle sector refers to the thickest step, 15 mm thick, of the ladder. The 58 MeV protons of the CATANA beam have insufficient energy to exit after passing through the thickness of the A12 range shifter and 15 mm of PVC. Moreover, border effects due to the non-orthogonality of the ladder with respect to the beam axis and the unavoidable divergence of the beam caused by the use of range shifters are visible in the radiography. The void pixels within the spot correspond to pixels where the range measurement statistics is too low. Many of these pixels are aligned along the same row or column, suggesting a correlation to low efficiency of the tracker in those areas. Two different 3D perspectives of the radiography are shown in **Figure 10(a)** and **(b)**. The last step in the analysis is the calculation of the relation between the measured range and the ΔE energy lost by the particles. The ΔE calculation must also take into account the energy lost by the particles in the PSD, which is placed between the target and the RRD. Since the sensitive areas of both detectors consist of 500 μm layers of SciFi, the PSD can be considered as an extension of the RRD. The residual proton range in the PSD and RRD was simulated as a function of the particle initial energy in the tracker E.

The range values thus obtained were fitted to the power law reported below in the equation, where R is the particle range in the RRD and PSD, expressed as the number of layers, and the resulting fit parameters are A = −0.191 ± 0.311 and B = 0.0370 ± 0.0006 (R - square = 0.998). Therefore, the energy loss ΔE can be easily calculated as

$$\Delta E[MeV] \;=\; 58 - \left(\frac{R-A}{B}\right)^{1/1.75}$$

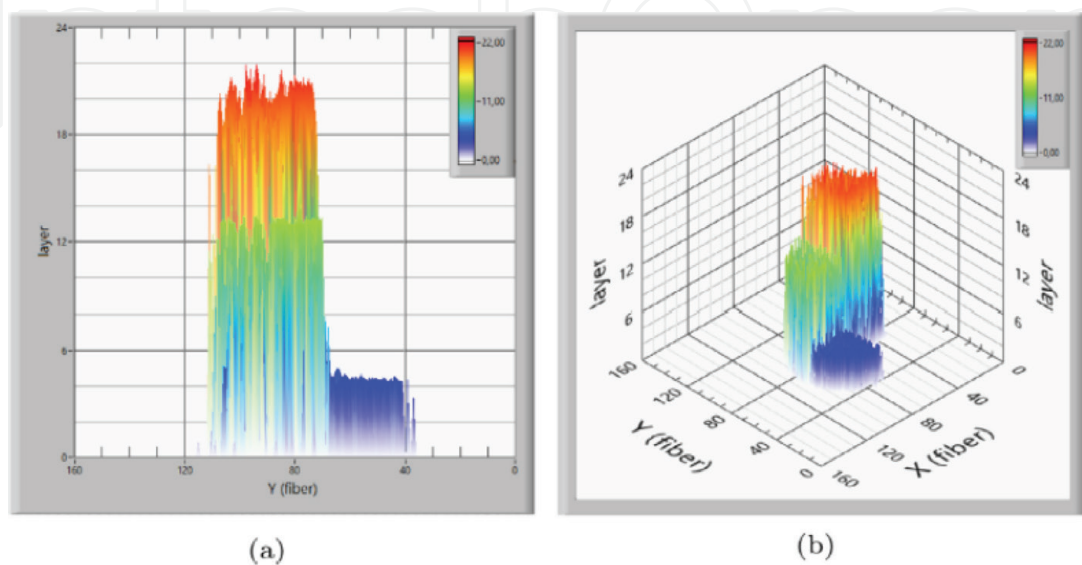The final radiography obtained after applying the energy-range conversion formula is shown in **Figure 11**.

(a)   (b)

Figure 10.
Two different perspectives of the 3D representation of the radiography: (a) lateral view and (b) isometric perspective.
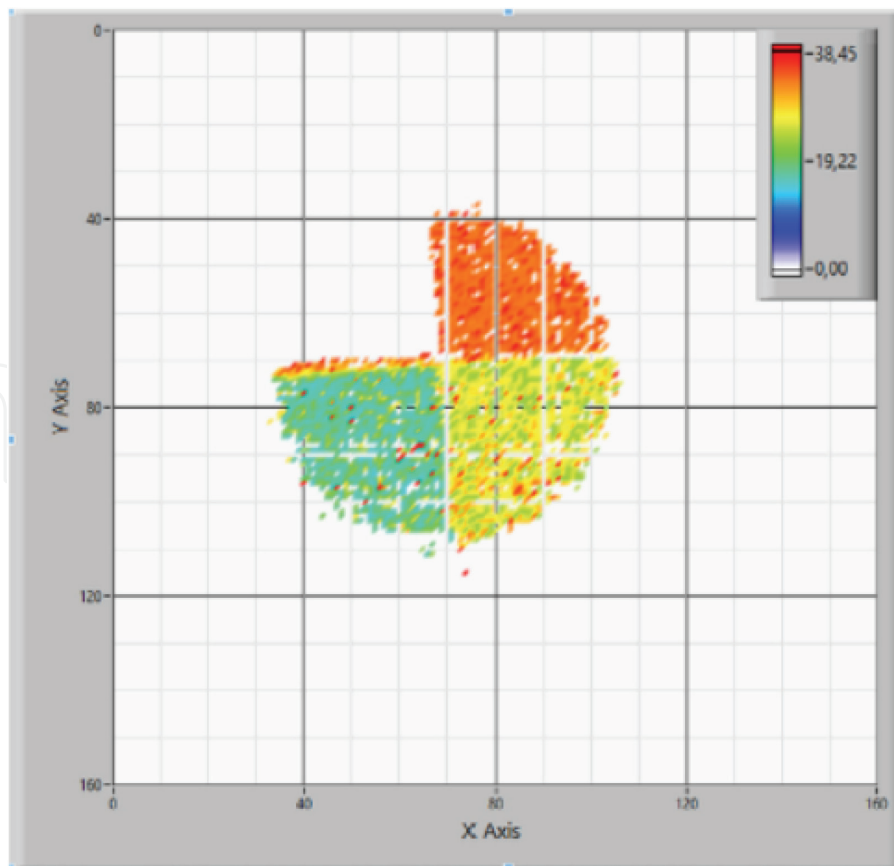
Figure 11.
The radiography of the ladder with A12 range shifter expressed in energy loss.

7. Radiograph data analysis

As mentioned earlier, radiography images reconstructed from range measurements are subject to some limitations: (i) lack of knowledge of the effective paths of the particles crossing the phantom because only one PSD was used. In this case, particle trajectories cannot be corrected according to the effect of Multiple Coulomb; (ii) further beam divergence was introduced by the tolerances in the alignment of the target, not exactly placed at isocenter and perpendicular to the incident beam direction. The reduction of the error in the calculus of the target thickness is obtained by the data filtering of range measurements. From the simulations, protons with an initial energy of 58 MeV crossing A12 range shifter, the target and the tracker, and stopping in the RRD have a maximum range straggling of σ_{str} = 0.4 mm, which already includes the effects of initial energy spread (0.3 MeV). So, in a region of interest (ROI) corresponding to a homogeneous quarter of the target, a range of measurements around the expected value from the simulation can be selected plus or minus two layers (equal to six times σ_{str}).

Subtracting the square of the maximum range straggling value of σ_{str} = 0.4 mm from the standard deviation of range measurements, it is again possible to find the a priori range resolution of about 170 μm. These mean range values can be converted into proton energy loss and subsequently into energy loss.

8. Future developments

The combined use of a pencil beam facility and the radiographic system, presented in this chapter, could allow the development of a faster real-time
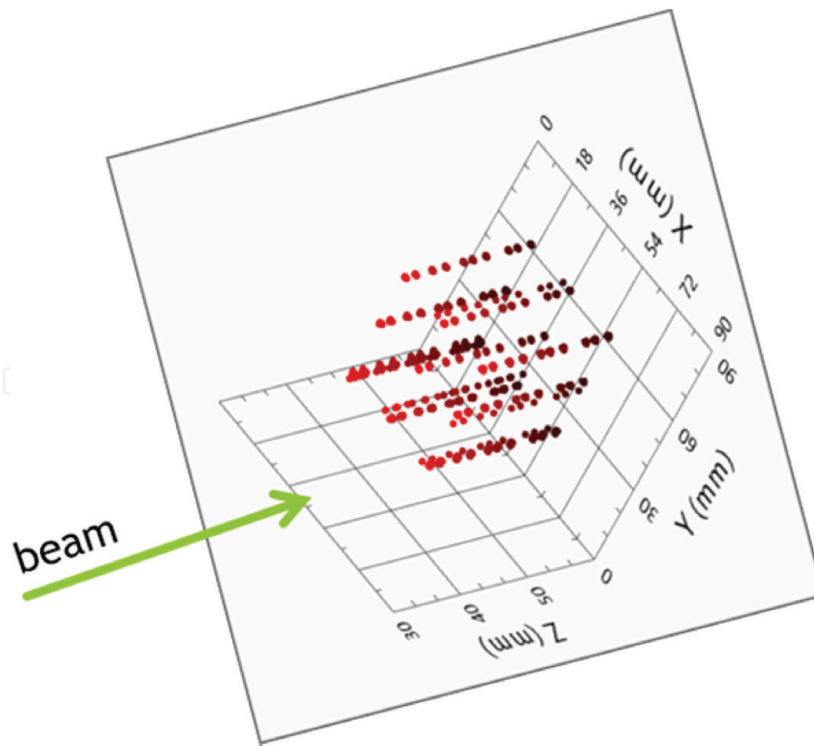
Figure 12.
The real-time reconstructed pattern. The x and y for each point are measured by the PSD. The z is the range measured by the RRD. The color is proportional to the measured fluence.

radiographic technique. Furthermore, the acquired radiography will be spatially correlated with the treatment plan applied to the patient. Exploiting the features of the described proton imaging system, a new method of quantifying treatment plan quality will be investigated.

A demonstrative measurement has been performed at CNAO in Pavia. A simple pattern of point in the field of view of the radiographic system, presented in this chapter, was covered by the pencil beam. The same pattern was modulated in energy, in the range of energy compatible with the range in the RRD, in order to obtain a 3D matrix. Each point in the matrix was covered by the pencil beam in one spill delivering a fixed dose, up to 10^9 protons per spill. The PSD measured the centroid, the FWHM and the fluence of the beam delivered in each position. The RRD measured the centroid, the FWHM of the range of the protons delivered in each spill. **Figure 12** shows the real-time reconstructed pattern.

The results demonstrate the potentiality of the system. Accurate measurements will be performed in order to refine these statements in a quantitative way at TIFPA in a treatment room. In these future tests, a calibrated phantom will be used for the measurement.

The definition of the optimal parameters for the radiography, e.g., beam energy and fluence to be chosen in order to obtain the required spatial and density resolution will allow the definition of the specifications for the design of the final detectors.

9. Conclusions

This chapter presents the design and characterization of an innovative imaging system for charged particle beam based on SciFi. The system consists of a position-sensitive detector and a residual range detector. Both prototypes, with a sensitive area of 90 × 90 mm^2, have cutting-edge performances, which distinguish them from

all other devices designed for the purposes considered in this chapter. In addition, improvements in the DAQ chain and the use of SiPM arrays make possible the use of the PSD as a beam monitoring and quality assurance system, by measuring real time the center and the shape of the spot, the fluence, and residual energy of the beam. The verification of this feature was investigated and demonstrated in beam tests. The performance of the PSD and RRD was tested at CATANA proton therapy facility with energies up to 58 MeV. Moreover, Monte Carlo simulations of the RRD detector response and the radiography of a calibrated target were measured by the system. From the analysis of the results and by a comparison with data from simulations, the architecture and the technology were validated.

Tests at CNAO and TIFPA validated the functionality of these devices with active beam shaping systems using protons with energies up to 250 MeV. Future developments concern the real-time qualification of a treatment plan and the comparison of the results with those provided by the official dose delivery system. Furthermore, the feasibility of a real-time radiography exploiting pencil beam will be tested.

Author details

Domenico Lo Presti[1,2]*, Giuseppe Gallo[1,2], Danilo Luigi Bonanno[2], Daniele Giuseppe Bongiovanni[2], Fabio Longhitano[2] and Santo Reito[2]

1 Department of Physics and Astronomy, University of Catania, Catania, Italy

2 Istituto Nazionale di Fisica Nucleare, Catania, Italy

*Address all correspondence to: domenico.lopresti@ct.infn.it

IntechOpen

References

[1] Poludniowski G, Allinson N, Evans P. Proton radiography and tomography with application to proton therapy. The British Journal of Radiology. 2015;**88**(1053):20150134

[2] Schneider U, Pedroni E. Proton radiography as a tool for quality control in proton therapy. Medical Physics. 1995;**22**(4):353-363

[3] Gallo G, Lo Presti D, Bonanno D, Longhitano F, Bongiovanni D, Reito S, et al. QBeRT: An innovative instrument for qualification of particle beam in real-time. Journal of Instrumentation. 2016;**11**(11):C11014

[4] Lo Presti D. Detector based on scintillating optical fibers for charged particle tracking with application in the realization of a residual range detector employing a read-out channels reduction and compression method. INFN Patent No. WO2013186798; 2013

[5] Cirrone GAP et al. A 62-MeV proton beam for the treatment of ocular melanoma at Laboratory Nazionali del SUD–INFN. IEEE Transactions on Nuclear Science. Jun. 2004;**51**(3):860-865

[6] SGC Products. Scintillating Fiber Webpage. http://www.crystals.saint-gobain.com/products/scintillating-fiber

[7] Lo Presti D, Bonanno D, Longhitano F, Pugliatti C, Aiello S, Cirrone G, et al. A real-time, large area, high space resolution particle radiography system. Journal of Instrumentation. 2014;**9**(06):C06012

[8] Lo Presti D, Aiello S, Bonanno D, Cirrone GAP, Leonora E, Longhitano F, et al. OFFSET: Optical Fiber Folded Scintillating Extended Tracker. Nuclear Instruments and Methods in Physics Research Section A: Accelerators, Spectrometers, Detectors and Associated Equipment. 2014;**737**:195-202

[9] Lo Presti D, Bonanno D, Longhitano F, Bongiovanni D, Russo G, Leonora E, et al. Design and characterisation of a real time proton and carbon ion radiography system based on scintillating optical fibres. Physica Medica. 2016;**32**(9):1124-1134

[10] Lo Presti D et al. An innovative proton tracking system for qualification of particle beam in real-time. IEEE Transactions on Radiation and Plasma Medical Sciences. 2017;**1**(3):268-274. DOI: 10.1109/TRPMS.2017.2690842